

Article

Microwave Drying Kinetics of Chromium-Rich Electroplating Sludge

Jian Zhang, Zhiwei Peng *, Guanwen Luo, Ran Tian and Mingjun Rao 

School of Minerals Processing and Bioengineering, Central South University, Changsha 410083, China

* Correspondence: zwpeng@csu.edu.cn; Tel.: +86-731-8887-7656

Abstract: Chromium-rich electroplating sludge (CRES) is a hazardous solid waste with a high content of moisture requiring efficient drying before subsequent treatment. In this study, the microwave drying kinetics of CRES were examined. The results showed that CRES had good microwave absorptivity, contributing to a much shorter drying time and better drying performance compared with conventional drying. In comparison with conventional drying at 105 °C, the time of microwave drying at 600 W for total moisture removal was reduced by 98.5%. Compared to load mass and particle size, microwave power played a more important role in microwave drying. Based on the kinetics analysis, the microwave drying process of CRES could be divided into three successive stages, in which the drying rates were limited by external diffusion (before 110 s), both external diffusion and chemical reaction (between 110 s and 160 s), and chemical reaction (after 160 s), respectively. The Danish model was found to have the best fit with the microwave drying process of CRES.

Keywords: microwave drying; electroplating sludge; chromium hydroxide; permittivity; kinetic model

1. Introduction

In China, approximately 4 billion cubic meters of electroplating wastewater are produced every year [1] and 10 million tons of electroplating sludge are produced [2,3]. Because electroplating sludge meets the standards of Article 17 and Article 21 of the National Catalogue of Hazardous Wastes of China [4], its efficient and harmless disposal is deemed an important task in the electroplating industry.

Untreated electroplating sludge has a pretty high moisture content, up to 80 wt% [5,6]. Drying electroplating sludge can reduce its quantity and volume with the retention of heavy metal ions. Mechanical pressure filtration dehydration is widely used because its energy consumption is only 3–5% of thermal drying. However, the moisture content of the filter cake after ultra-high-pressure dehydration is still in the range 40–60 wt% [5,7] because the residual water, including the crystal water from chromium hydroxide, is difficult to remove from the sludge [8]. Further dewatering of the sludge by thermal drying will enable lower cost and higher convenience of management [9] although some applications, such as clay brick preparation, prefer using sludge with a certain amount of moisture as the raw material [10]. Therefore, it is of great significance to develop efficient thermal drying technology for the disposal of electroplating sludge.

Compared with traditional thermal drying methods, microwave drying has many advantages, such as higher heating efficiency, owing to the selective and volumetric thermal effects as well as the non-thermal effect of microwave energy [11,12]. By taking advantage of the strong microwave absorptivity of water molecules, microwave drying technology has been widely used in the pre-treatment of various sludges, including hazardous chromium-rich electroplating sludge (CRES) [13–16]. Microwave drying of these sludges is characterized by rapid drying, fast process start-up and shutdown, small carbon footprint, etc., in spite of limited treatment capacity [17]. This is because microwave drying performance highly depends on the microwave response characteristics and drying



Citation: Zhang, J.; Peng, Z.; Luo, G.; Tian, R.; Rao, M. Microwave Drying Kinetics of Chromium-Rich Electroplating Sludge. *Metals* **2023**, *13*, 87. <https://doi.org/10.3390/met13010087>

Academic Editor: Chih-Ming Chen

Received: 26 November 2022

Revised: 21 December 2022

Accepted: 23 December 2022

Published: 30 December 2022



Copyright: © 2022 by the authors. Licensee MDPI, Basel, Switzerland. This article is an open access article distributed under the terms and conditions of the Creative Commons Attribution (CC BY) license (<https://creativecommons.org/licenses/by/4.0/>).

rate-limiting step of the target. However, no relevant systematic studies of CRES have been reported [16].

The purpose of this study was to explore the microwave drying kinetics of CRES, with a focus on the influence of the microwave response characteristics of the sludge and the determination of the drying rate-limiting step. The findings can provide a useful guidance for electroplating sludge pretreatment.

2. Experimental

2.1. Materials

The sample of CRES was taken from a chromium plating enterprise in the Xi'an electroplating industrial park, China. It was produced by the purification of electroplating wastewater containing Cr (VI) using several chemical reagents, including sodium pyrosulfite ($\text{Na}_2\text{S}_2\text{O}_5$) and sodium hydroxide (NaOH), successively before pressure filtration. The moisture content of the CRES sample was 45.72% with a volume shrinkage of 40% after the moisture in the sample was completely removed. The photo of the CRES sample before drying is shown in Figure 1.



Figure 1. Photo of CRES.

2.2. Experimental Procedure

2.2.1. Particle Size Distribution and Corresponding Moisture Content Distribution

After crushing and mixing the as-received sludge sample using a small rod mill rotating at 15 r/min for 10 min, 1000 g of the sample was taken and separated for determining particle size distribution using several standard sieves (Shaoxing Jinhang Instrument Co., Ltd., Shaoxing, China). After separation, the samples with different particle size fractions were dried in an oven at 105 °C for 24 h to calculate the moisture contents separately [18].

2.2.2. Chemical Composition and Phase Analysis

The dried sludge sample was used for chemical composition analysis. Specifically, the content of Cr was measured by ammonium ferrous sulfate titration. The contents of Al, P, and Si were measured using an inductively coupled plasma atomic emission spectrometer (Optima 8000DV, PerkinElmer Inc., Waltham, MA, USA). The content of S was measured using a carbon and sulfur analyzer (CS844, LECO, St. Joseph, MI, USA). The content of Cl was measured by the turbidity method. The contents of other elements were measured using an atomic absorption spectrometer (Pinaade 900T, PerkinElmer Inc., Waltham, MA, USA). The phase composition of the sample was measured using an X-ray diffraction spectrometer (XRD; D8 Advance, Bruker, Karlsruhe, Germany). For further analysis, the Raman spectrum of the sample was determined using a Raman spectrometer (BWS475-785S, B&W Tek, Inc., Newark, NJ, USA). The thermogravimetry-differential thermogravimetry-differential scanning calorimetry (TG-DTG-DSC) analysis of CRES was carried out using a simultaneous thermal analyzer (STA449F3, Netzsch, Selb, Germany) with a heating rate of 10 °C/min in air and flow rate of 20 mL/min.

2.2.3. Permittivity Measurement

Generally, the microwave drying performance of a dielectric material is directly dependent on its microwave response, which can be determined by measuring its complex relative permittivity [19]. In this study, the permittivity measurements of the CRES samples with different moisture ratios were carried out using the coaxial waveguide method. The powdered CRES samples were molded firstly with the addition of paraffin as the binder. They were mixed with paraffin in a mass ratio of 7/3 to form mixtures that were heated and evenly stirred before being placed into a precise mold to cure. After loading in a waveguide sampler, the permittivity values of the samples were measured using a vector network analyzer (E8362C, Agilent Technology Co., Ltd., Palo Alto, CA, USA).

2.2.4. Microwave Drying

The microwave drying experiments were conducted using a microwave thermogravimetric furnace operated at 2.45 GHz with a maximum power of 2.4 kW (CY-TH1200C-M, Hunan Change Microwave Technology Co., Ltd., Changsha, China), as shown in Figure 2. Note that an extra heating unit was equipped at the top of the furnace to prevent condensation and the backflow of water vapor during drying.

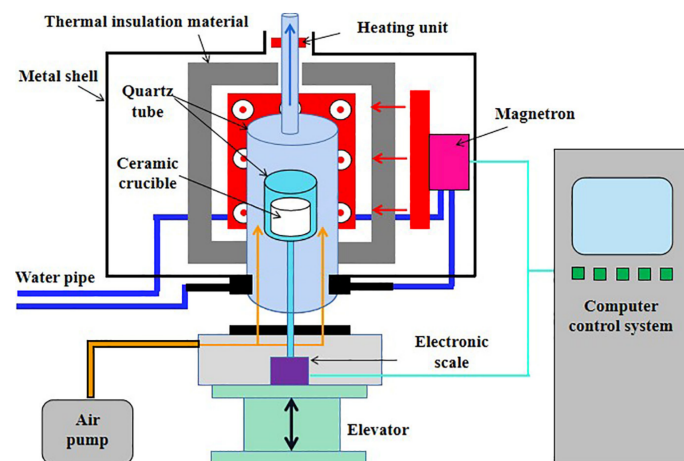


Figure 2. Schematic illustration of microwave thermogravimetric furnace.

During the microwave drying experiments, air was purged at 400 mL/min for drying. The samples, loaded in a ceramic crucible with an internal diameter of 34 mm and a height of 40 mm, were dried with constant microwave power and the weight losses were recorded every 10 s until the samples were completely dried. Note that constant-power drying rather than constant-temperature drying was applied in this study because there is often some temperature difference inside a thick material layer. This method has also been used in the literature [13,20]. For temperature measurement during the experiments, microwave was turned off immediately after drying for a certain time before inserting a thermometer into the material layer. This procedure was repeated 3 times and the average values were used.

2.2.5. Conventional Drying

For comparison with microwave drying, the conventional drying experiments were performed using a muffle furnace (DHG-9070A, Shanghai Jinghong Laboratory Equipment Co., Ltd., Shanghai, China). The samples, loaded in a ceramic crucible of the same size as that used in microwave drying, were transferred to the furnace for drying at the target temperature for different periods of time. At regular intervals, the crucible was taken out and weighed quickly using an electronic scale to determine the drying rate.

2.2.6. Determination of Drying Kinetics

Equations for Calculation of Drying Parameters

For calculation of drying parameters, the moisture content on the dry basis should be firstly determined, as given by [20]

$$M_t = \frac{W_t - W_d}{W_d} \quad (1)$$

where M_t is the moisture content on the dry basis, wt%; W_t is the residual mass, g; and W_d is the mass on the dry basis, g. By ignoring the equilibrium moisture content of the raw materials on the dry basis, the moisture ratio could be determined using the following equation [20].

$$M_R = \frac{M_t}{M_0} \quad (2)$$

where M_R is the moisture ratio, dimensionless, and M_0 is the initial moisture content on the dry basis, wt%. The equation for calculating the drying rate is expressed as [20]

$$R_D = \frac{M_t - M_{t+\Delta t}}{\Delta t} \quad (3)$$

where R_D is the drying rate, s^{-1} , and Δt is the interval time, s. Whether the drying process is limited by diffusion or the decomposition reaction of chromium hydroxide, the drying rate is proportional to the moisture content. Therefore, the drying rate constant is expressed as R_D/M_R .

To quantitatively analyze the potential influence of diffusion on drying, the diffusion rate of the material under ideal conditions could be expressed by Fick's second law [21], given by

$$\frac{\partial C}{\partial t} = D \frac{\partial^2 C}{\partial x^2} \quad (4)$$

where c is the concentration of reactants, kg/m^3 ; t is the reaction time, s; D is the diffusion coefficient, m^2/s ; and x is the diffusion distance, m. According to the equation, the diffusion rate is directly proportional to the square of the diffusion distance. The drying process usually involves the exchange of water molecules and air, so the empirical formula, Equation (5), could be used for estimating the binary gas diffusion coefficient [22].

$$D = \frac{0.0101 \times T^{1.75} \left(\frac{1}{M_A} + \frac{1}{M_B} \right)^{\frac{1}{2}}}{P \left[(\sum \nu_A)^{1/3} + (\sum \nu_B)^{1/3} \right]^2} \quad (5)$$

where P is the total pressure, Pa; T is the thermodynamic temperature, K; M_A and M_B are the molar masses of components A (air) and B (H_2O), g/mol; and $\sum \nu_A$ and $\sum \nu_B$ are the molecular diffusion volumes of A and B, cm^3/mol . For the drying process of CRES limited by external diffusion, the drying rate constant should obey the following relationship.

$$\frac{R_D}{M_R} \propto \delta^{-2} T^{1.75} \quad (6)$$

where R_D/M_R is the drying rate constant, s^{-1} , and δ is material layer thickness, mm.

Kinetic Models

Both semi-theoretical and semi-empirical models can be used for analysis of thin-layer drying kinetics [20,23–26]. Considering the influence of temperature variation on the early and late stages of the microwave drying process, a modified Page model and

three improved models in Table 1, which were also frequently used in the aforementioned literature, were selected for investigating the drying kinetics of CRES.

Table 1. Models of thin-material-layer drying kinetics.

No.	Model	Equation	Reference
1	Modified Page	$M_R = \exp(-kt^n)$	[20,23]
2	Midilli	$M_R = a \cdot \exp(-kt^n) + bt$	[24]
3	Balbay and Sahin	$M_R = (1-a) \cdot \exp(-kt^n) + b$	[25]
4	Danish	$M_R = \exp(-kt^n) + b$	[26]

Note: t is the time, s ; k is the drying coefficient, s^{-1} ; a , b , c , and n are the dimensionless coefficients.

Except for the commonly used determination coefficient (R^2), the residual squared sum (RSS) and chi-squared test value (χ^2) were employed for the evaluation of fitting results, given by Equations (7) and (8) [20], respectively.

$$RSS = \sum_{i=1}^N (M_{R1,i} - M_{R2,i})^2 \quad (7)$$

$$\chi^2 = RSS / (N - m) \quad (8)$$

where $M_{R1,i}$ is the moisture ratio of the i -th experiment, dimensionless; $M_{R2,i}$ is the moisture ratio predicted by the drying kinetic model, dimensionless; N is the number of data points of moisture ratio, dimensionless; and m is the number of parameters in the model, dimensionless. The Akaike's information criterion (AIC , dimensionless) has been widely used to select the best prediction model from multiple candidate models [27]. When the error of the model obeys the normal distribution, AIC could be determined by

$$AIC = 2m + N \ln(RSS/N) \quad (9)$$

For fitting the drying kinetic models, the software Origin 9 (OriginLab Co., Northampton, MA, USA) was used.

3. Results and Discussion

3.1. Physical and Chemical Properties

The particle size distribution and corresponding moisture content distribution of CRES are shown in Figure 3. It shows that 39.60%, 17.23%, and 25.33% of the sludge particles had the size fractions of 0.15–0.3 mm, 0.3–0.6 mm, and 0.6–1.25 mm, respectively. As the particle size changed, the moisture content varied slightly between 43.65 wt% and 45.46 wt%. It indicated that there was no strong relationship between particle size and moisture content.

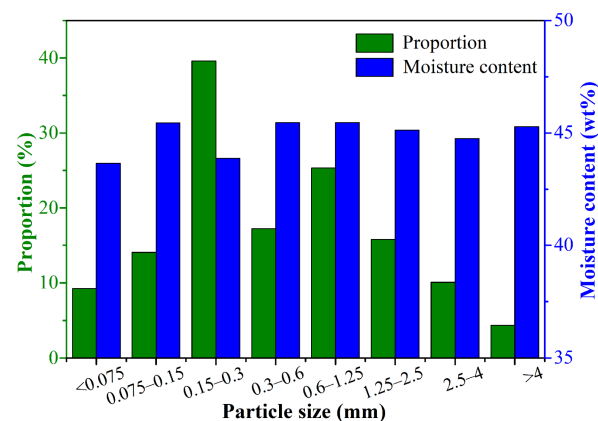


Figure 3. Particle size distribution and corresponding moisture content distribution of CRES.

The chemical composition and XRD pattern of CRES are shown in Table 2 and Figure 4, respectively. Although the sludge had a high content of chromium, it had low crystallinity. The main crystalline phases were probably chromium oxyhydroxide/hydroxide and oxide, as revealed in Figure 4.

Table 2. Chemical composition of CRES.

Element	Cr	Fe	Ca	S	Cu	Zn	Pb	Ni
Content (wt%)	36.85	4.64	2.32	2.03	0.24	0.24	0.22	0.03
Element	Na	Cl	Mg	Al	Si	P	K	
Content (wt%)	0.03	0.01	0.31	0.17	0.22	0.08	0.01	

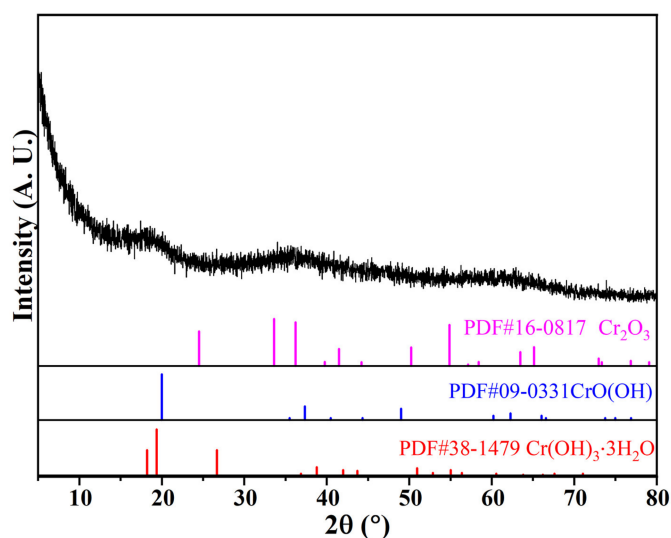


Figure 4. XRD pattern of CRES.

According to the Raman spectrum of the dried CRES sample in Figure 5, it mainly contained chromium oxyhydroxide (α -CrO(OH)) and Cr₂O₃ [28]. It was reported that chromium hydroxide in either crystalline or amorphous form underwent a decomposition reaction at 105 °C [8], generating Cr₂O₃ during drying. In other words, crystal water in the sludge could be removed during the drying process.

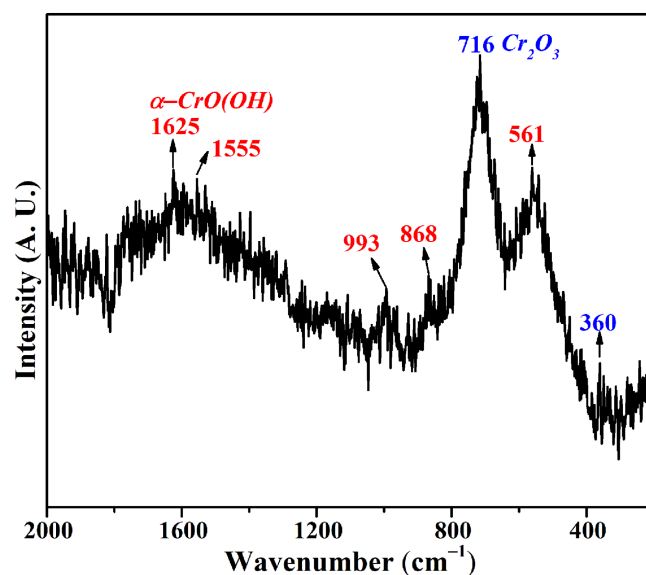


Figure 5. Raman spectrum of CRES.

The TG-DTG-DSC analysis of CRES is shown in Figure 6. The temperature corresponding to the maximum weight loss rate was 99.2 °C and the temperature corresponding to the maximum heat absorption was 106.1 °C. The shaded zone indicates that the sludge drying mainly took place below 130 °C.

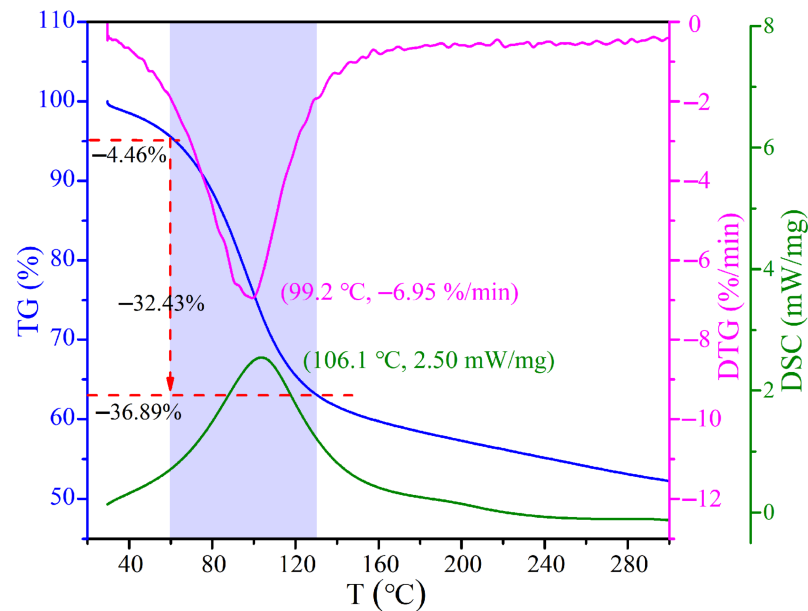


Figure 6. TG-DTG-DSC curves of CRES in air.

3.2. Microwave Response Characteristics of CRES

The microwave response characteristics of CRES could be determined by the values of permittivity of CRES with different moisture ratios, as shown in Table 3. It was found that the complex relative permittivity of the sludge decreased with decreasing moisture ratio. Meanwhile, the dielectric loss angle tangent declined significantly. As a result, the microwave penetration depth of the sludge increased from only 34.72 mm to as large as 460.20 mm with the decrease of moisture ratio from 1 to 0. It proved the dominant role of water molecules in controlling the microwave absorptivity of the sludge. Obviously, this feature would favor the selective heating of water in the sludge and, thus, rapid water removal under microwave irradiation.

Table 3. Variation of permittivity of CRES with moisture ratio.

M_R	ϵ'_r	ϵ''_r	$\tan\delta_\epsilon$	D_p (mm)
1.000	4.574	1.705	0.373	34.72
0.474	3.299	0.513	0.156	96.69
0.374	2.961	0.347	0.117	135.25
0.256	2.590	0.312	0.120	140.70
0	2.687	0.097	0.036	460.20

Note: ϵ'_r is the real part of the complex relative permittivity (relative dielectric constant), dimensionless; ϵ''_r is the imaginary part of the complex relative permittivity (relative dielectric loss factor), dimensionless; $\tan\delta_\epsilon$ is the dielectric loss angle tangent, dimensionless; and D_p is the microwave penetration depth, mm.

3.3. Microwave Drying Kinetics

The variation of moisture ratio of CRES with time in microwave drying is shown in Figure 7. Because the raw sludge had a strong microwave response, the rate of microwave drying was much higher than that of conventional drying. For instance, compared with conventional drying at 105 °C, the time of microwave drying at 600 W for total moisture removal was reduced by 98.5%.

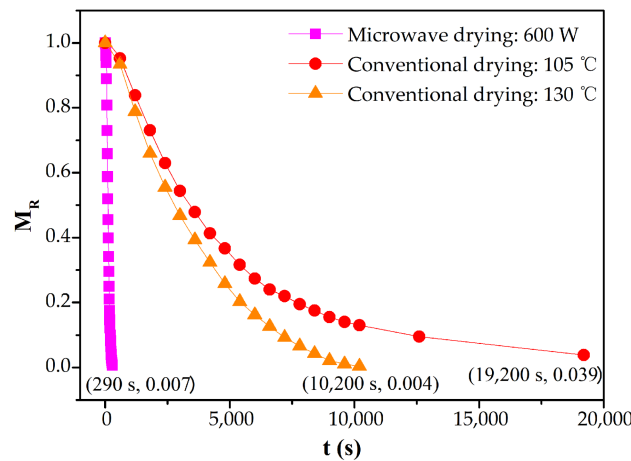


Figure 7. Variations of moisture ratio of CRES with time in the microwave and conventional drying processes.

The effects of microwave power on the moisture ratio and drying rate of CRES were assessed by fixing the CRES load mass of 10 g and particle size fraction of 0.6–1.25 mm. As shown in Figure 8 and Table 4, microwave power had a significant effect on the moisture ratio and drying rate of CRES. In particular, when the microwave power increased from 600 W to 1200 W, the moisture ratio declined more rapidly with increasing time and the average drying rate increased from 0.00297 s^{-1} to 0.00491 s^{-1} .

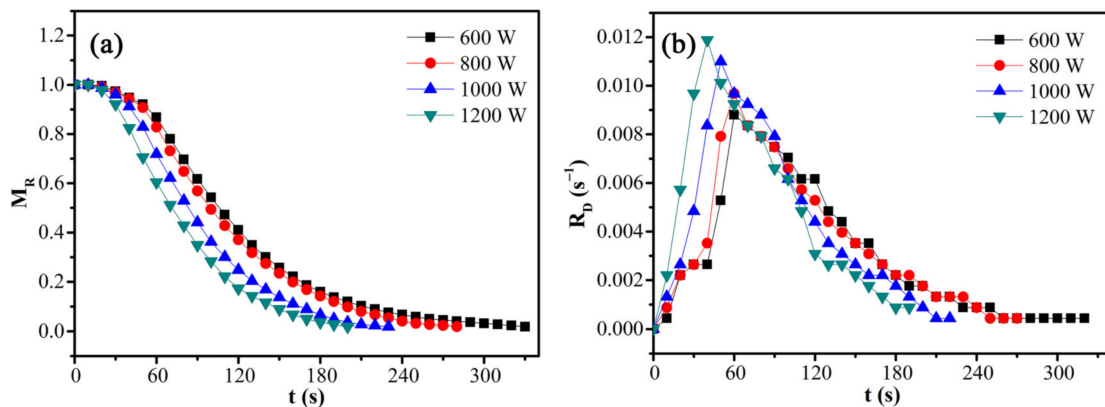


Figure 8. Effects of microwave power on the (a) moisture ratio and (b) drying rate of CRES in the microwave drying process.

Table 4. Variations of microwave drying characteristics of CRES with microwave power.

Microwave Power (W)	600	800	1000	1200
Average drying rate (s^{-1})	0.00297	0.00350	0.00427	0.00491
Maximum drying rate (s^{-1})	0.00870	0.00957	0.0109	0.0117
Temperature at the maximum drying rate ($^{\circ}\text{C}$)	80.1	81.8	83.9	84.2
End-point temperature ($^{\circ}\text{C}$)	113.7	113.3	113.5	115.3

The effects of load mass on the moisture ratio and drying rate of CRES were studied by fixing the microwave power of 600 W and CRES particle size fraction of 0.6–1.25 mm, as shown in Figure 9 and Table 5. When the load mass increased from 7.5 g to 12.5 g, the average drying rate increased slightly from 0.00282 s^{-1} to 0.00339 s^{-1} . However, when the load mass increased continuously, it changed very slightly. The average drying rate did not decrease with increasing load mass because the temperature increased with load mass, as shown in Figure 10. When the load mass exceeded 12.5 g, the increase of temperature

was not obvious. It explained the increase of the maximum drying rate when the load mass increased from 7.5 g to 10 g. As shown in Table 5, the maximum drying rate also varied around 0.008 s^{-1} when the load mass was no more than 12.5 g. With further increases in load mass, the rate declined clearly. This observation was mainly attributed to the rapid decrease of temperature difference between the sludge layers when the load mass increased from 7.5 g to 12.5 g, beyond which the temperature difference become much smaller (Figure 10).

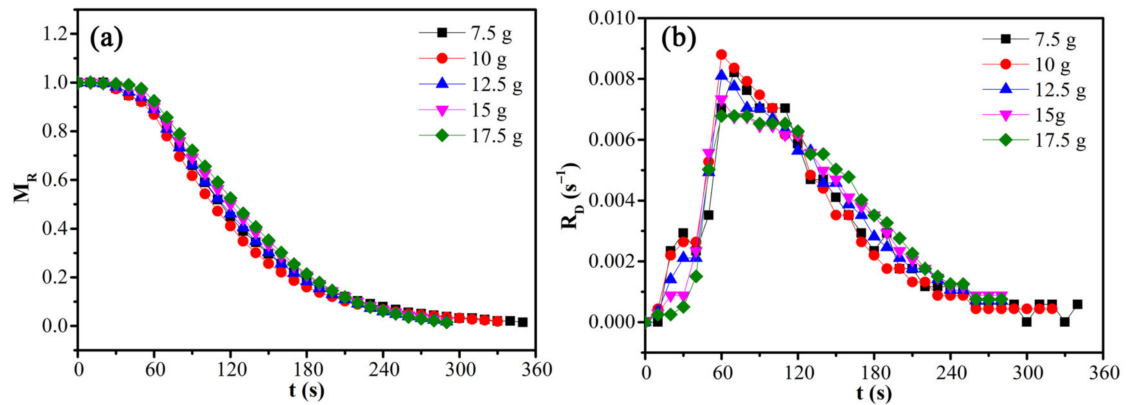


Figure 9. Effects of load mass on the (a) moisture ratio and (b) drying rate of CRES in the microwave drying process.

Table 5. Variations of microwave drying characteristics of CRES with load mass.

Load Mass (g)	7.5	10	12.5	15	17.5
Material layer thickness (mm)	7.80	10.39	12.99	15.59	18.19
Average drying rate (s^{-1})	0.00282	0.00297	0.00339	0.00339	0.00340
Maximum drying rate (s^{-1})	0.00812	0.00870	0.00800	0.00725	0.00671

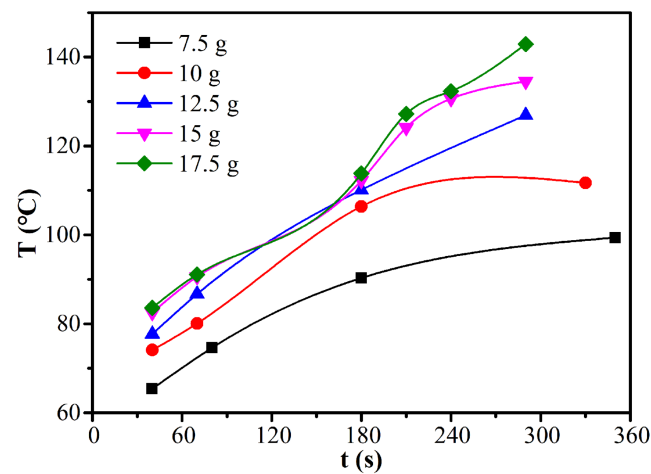


Figure 10. Effect of load mass on the temperature of CRES in the microwave drying process.

The effects of particle size on the moisture ratio and drying rate of CRES were evaluated by fixing the microwave power of 600 W and load mass of 12.5 g. As shown in Figure 11 and Table 6, the sludge particle size had little influence on the moisture ratio and drying rate of CRES. With the increase of particle size by several times, the drying rate increased minorly within the range of 12%.

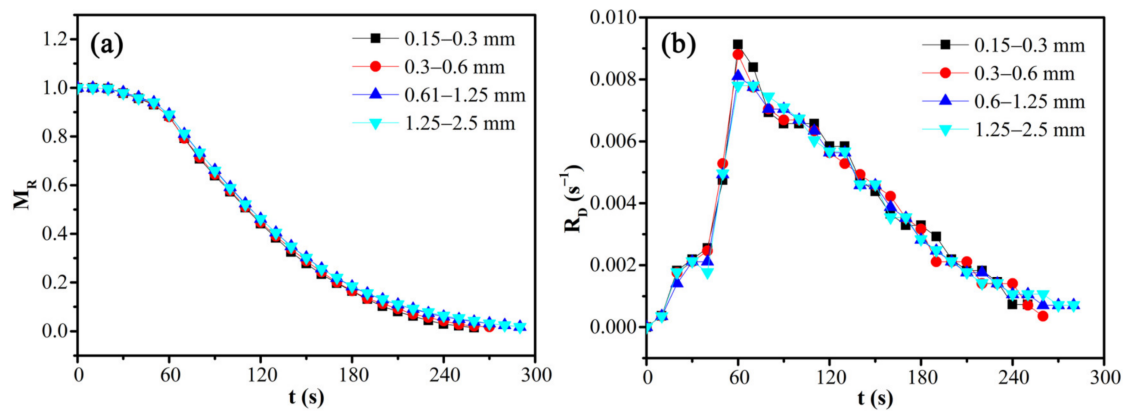


Figure 11. Effects of particle size on the (a) moisture ratio and (b) drying rate of CRES in the microwave drying process.

Table 6. Variations of microwave drying characteristics of CRES with particle size.

Particle Size (mm)	0.15–0.3	0.3–0.6	0.6–1.25	1.25–2.5
Average drying rate (s^{-1})	0.00379	0.00364	0.00339	0.00339
Maximum drying rate (s^{-1})	0.00912	0.00870	0.00800	0.00780
Temperature at maximum drying rate ($^{\circ}C$)	89.4	89.1	86.7	84
End-point temperature ($^{\circ}C$)	135.4	131.3	126.9	117.4

3.4. Analysis of the Rate-Limiting Step

The independence of the drying rate on sludge particle size showed that internal diffusion was not the rate-limiting step. The variations of drying rate constant with time and load mass are shown in Figure 12.

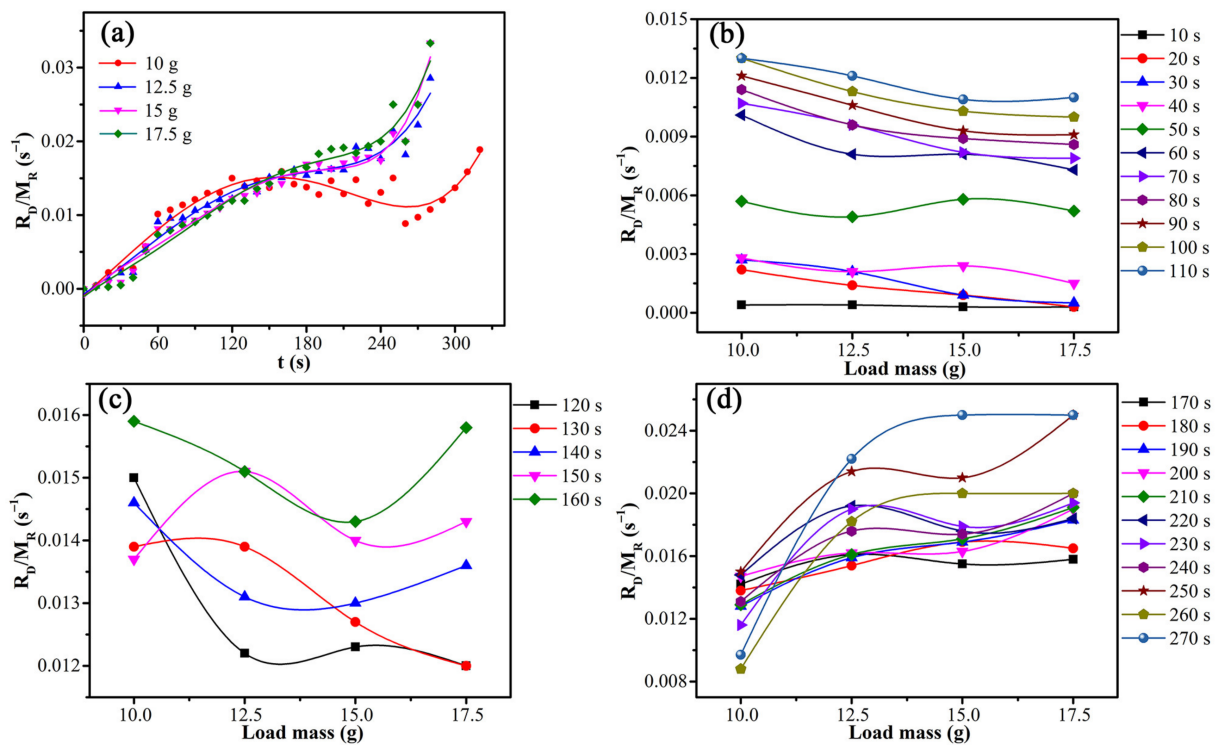


Figure 12. Variations of drying rate constant with time and load mass: (a) the entire process, (b) before 110 s, (c) 110 s–160 s, and (d) after 160 s.

According to Figure 12a, the microwave drying process of CRES could be roughly separated into three successive stages considering the variations of drying rate constant with time and load mass. Figure 12b shows that the drying rate constant was basically negatively correlated with the load mass before 110 s, agreeing with the dependence shown by Equation (6). Thus, in this stage, the drying process was limited by external diffusion. Figure 12c shows that there was no obvious correlation between the drying rate constant and load mass from 120 s to 160 s, indicating that the drying process was controlled by both external diffusion and chemical reaction. Figure 12d shows that the drying rate constant has no clear negative correlation with load mass after 160 s. Instead, it had a certain degree of positive correlation, which was qualitatively consistent with the Arrhenius formula. It indicated that the drying process was mainly controlled by chemical reactions.

3.5. Fitting of Kinetic Models

The fitting results of kinetic models for the microwave drying process of CRES are shown in Figure 13 and Table 7. It was found that the Danish model fit best with the drying data among the tested kinetic models, primarily due to its high correlation coefficient and smaller chi-squared test value when the load mass increased from 7.5 g to 17.5 g.

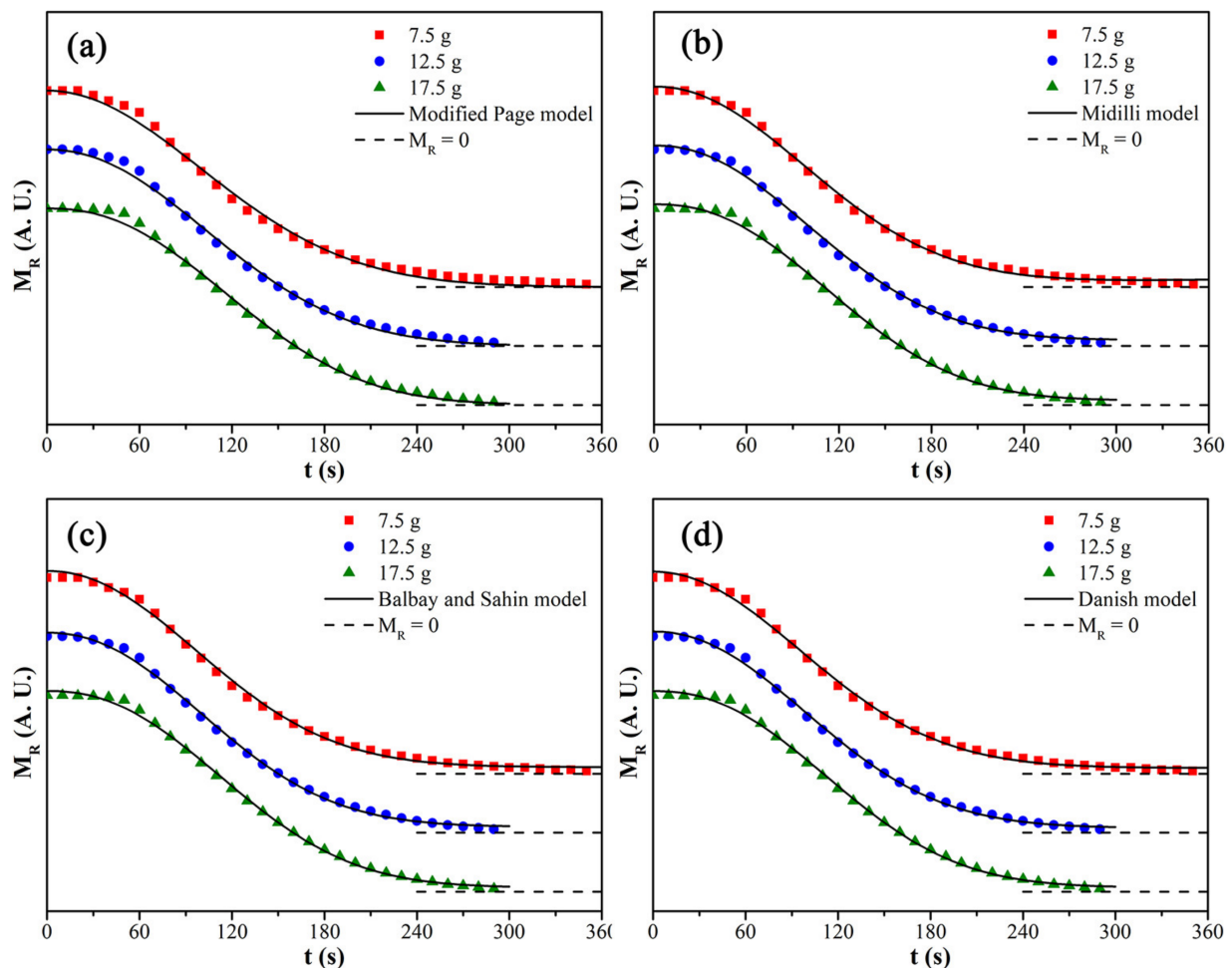


Figure 13. Fitting curves of different kinetic models: (a) modified Page model, (b) Midilli model, (c) Balbay and Sahin model, and (d) Danish model.

Table 7. Model fitting results of the microwave drying process.

Model	Load Mass (g)	Parameters	R^2	RSS	χ^2	AIC
Modified Page	7.5	$k = 0.00713, n = 2.00734$	0.996	0.01968	5.788×10^{-4}	−266.4
	12.5	$k = 0.00717, n = 2.11124$	0.997	0.01066	3.806×10^{-4}	−234.3
	17.5	$k = 0.00673, n = 2.30727$	0.998	0.00926	3.307×10^{-4}	−238.5
Midilli	7.5	$a = 1.01993, b = 1.04033 \times 10^{-4}, k = 4.04004 \times 10^{-5}, n = 2.06505$	0.998	0.00847	2.646×10^{-4}	−292.8
	12.5	$a = 1.02011, b = 9.60889 \times 10^{-5}, k = 3.01866 \times 10^{-5}, n = 2.11995$	0.998	0.00537	2.066×10^{-4}	−250.8
	17.5	$a = 1.02095, b = 7.14532 \times 10^{-5}, k = 1.18911 \times 10^{-5}, n = 2.28123$	0.999	0.00502	1.930×10^{-4}	−252.9
Balbay and Sahin	7.5	$a = 0.01243, b = 0.0342, k = 3.65816 \times 10^{-5}, n = 2.0911$	0.998	0.00751	2.348×10^{-4}	−297.1
	12.5	$a = 0.01169, b = 0.03036, k = 2.41858 \times 10^{-5}, n = 2.17321$	0.999	0.00528	2.030×10^{-4}	−251.4
	17.5	$a = -7.50411 \times 10^{-4}, b = 0.02087, k = 1.08217 \times 10^{-5}, n = 2.30206$	0.999	0.00504	1.937×10^{-4}	−252.7
Danish	7.5	$b = 0.02988, k = 4.65995 \times 10^{-5}, n = 2.04148$	0.998	0.00784	2.377×10^{-4}	−297.6
	12.5	$b = 0.0244, k = 3.1433 \times 10^{-5}, n = 2.11821$	0.999	0.00533	1.976×10^{-4}	−253.1
	17.5	$b = 0.02126, k = 1.06884 \times 10^{-5}, n = 2.30461$	0.999	0.00504	1.866×10^{-4}	−254.7

4. Conclusions

The microwave drying kinetics of CRES were investigated with a focus on the effects of microwave power, load mass, and particle size fraction of CRES on the microwave drying rate of CRES. It was demonstrated that CRES had strong microwave absorption, contributing to a much shorter drying time and better drying performance compared with conventional drying. In comparison with conventional drying at 105 °C, the time of microwave drying at 600 W for total moisture removal was cut by 98.5%. With the increase of microwave power from 600 W to 1200 W, the average drying rate increased from 0.00297 s^{−1} to 0.00491 s^{−1}. As the load mass increased from 7.5 g to 17.5 g, the average drying rate increased from 0.00282 s^{−1} to 0.00340 s^{−1}. When the particle size varied from 0.15–0.3 mm to 1.25–2.5 mm, the average drying rate decreased from 0.00379 s^{−1} to 0.00339 s^{−1}. Compared with other factors, microwave power played a more important role in microwave drying. The microwave drying process of CRES included three successive stages, whose drying rates were, respectively, limited by external diffusion (before 110 s), both external diffusion and chemical reaction (110 s–160 s), and chemical reaction (after 160 s). Among the examined kinetic models, the Danish model fit best with the microwave drying process of CRES.

Author Contributions: Conceptualization, formal analysis, writing—original draft, visualization, J.Z.; resources, writing—review and editing, supervision, Z.P.; investigation, G.L.; methodology, R.T.; validation, M.R. All authors have read and agreed to the published version of the manuscript.

Funding: This work was partially supported by the Science and Technology Planning Project of Hunan Province, China, under Grant 2019RS2008 and the Fundamental Research Funds for the Central Universities of Central South University under Grant 2022zzts0426.

Institutional Review Board Statement: Not applicable.

Informed Consent Statement: Not applicable.

Data Availability Statement: The data presented in this study are available on request from the corresponding author.

Conflicts of Interest: The authors declare that they have no known competing financial interest or personal relationships that could have appeared to influence the work reported in this paper.

References

1. Yan, K.; Liu, Z.; Li, Z.; Yue, R.; Guo, F.; Xu, Z. Selective separation of chromium from sulphuric acid leaching solutions of mixed electroplating sludge using phosphate precipitation. *Hydrometallurgy* **2019**, *186*, 42–49. [[CrossRef](#)]
2. Chen, M.; Zhou, J.; Zhang, J.; Zhang, J.; Chen, Z.; Ding, J.; Kong, F.; Qian, G.; Chen, J. Ferrite catalysts derived from electroplating sludge for high-calorie synthetic natural gas production. *Appl. Catal. A-Gen.* **2017**, *534*, 94–100. [[CrossRef](#)]
3. Weng, C.; Sun, X.; Han, B.; Ye, X.; Zhong, Z.; Li, W.; Liu, W.; Deng, H.; Lin, Z. Targeted conversion of Ni in electroplating sludge to nickel ferrite nanomaterial with stable lithium storage performance. *J. Hazard. Mater.* **2020**, *393*, 122296. [[CrossRef](#)] [[PubMed](#)]
4. Wu, N.; Zhang, X.; Zhang, X.; Li, Y.; Song, X.; Wang, S. Electrochemical processes for the treatment of hazardous wastes exemplified by electroplating sludge leaching solutions. *Water* **2021**, *13*, 1576. [[CrossRef](#)]
5. Rao, B.; Zhu, Y.; Yu, M.; Lu, X.; Wan, Y.; Huang, G.; Su, X.; Liu, X. High-dry dewatering of sludge based on different pretreatment conditions. *Process Saf. Environ. Prot.* **2019**, *122*, 288–297. [[CrossRef](#)]
6. Fujimori, T.; Hayashi, H.; Nakajima, K. Phosphorus speciation in sludge from nickel electroplating. *Mater. Trans.* **2017**, *58*, 1337–1340. [[CrossRef](#)]
7. Guo, B.; Tan, Y.; Wang, L.; Chen, L.; Wu, Z.; Sasaki, K.; Mechtcherine, V.; Tsang, D.C.W. High-efficiency and low-carbon remediation of zinc contaminated sludge by magnesium oxysulfate cement. *J. Hazard. Mater.* **2021**, *408*, 124486. [[CrossRef](#)]
8. Huang, Z.; Chen, C.; Xie, J.; Wang, Z. The evolution of dehydration and thermal decomposition of nanocrystalline and amorphous chromium hydroxide. *J. Anal. Appl. Pyrol.* **2016**, *118*, 225–230. [[CrossRef](#)]
9. Yenikaya, S.; Salihoglu, G.; Salihoglu, N.K.; Yenikaya, G. Microwave drying of automotive industry paint sludge. *J. Hazard. Toxic Radioact. Waste* **2018**, *22*, 04018015. [[CrossRef](#)]
10. Pérez-Villarejo, L.; Martínez-Martínez, S.; Carrasco-Hurtado, B.; Eliche-Quesada, D.; Ureña-Nieto, C.; Sánchez-Soto, P.J. Valorization and inertization of galvanic sludge waste in clay bricks. *Appl. Clay Sci.* **2015**, *105*, 89–99. [[CrossRef](#)]
11. Sun, J.; Wang, W.; Yue, Q. Review on microwave-matter interaction fundamentals and efficient microwave-associated heating strategies. *Materials* **2016**, *9*, 231. [[CrossRef](#)]
12. Wu, Y.; Yan, B.; Yang, Y.; Zhu, H.; Huang, K. Accordion microwave oven for uniformity and efficiency heating. *Int. J. RF Microw. Comput.-Aided Eng.* **2019**, *30*, 22190. [[CrossRef](#)]
13. Guo, J.; Zheng, L.; Li, Z. Microwave drying behavior, energy consumption, and mathematical modeling of sewage sludge in a novel pilot-scale microwave drying system. *Sci. Total Environ.* **2021**, *777*, 146109. [[CrossRef](#)]
14. Eom, H.; Jang, Y.H.; Lee, D.Y.; Kim, S.S.; Lee, S.M.; Cho, E.M. Optimization of a hybrid sludge drying system with flush drying and microwave drying technology. *Chem. Eng. Res. Des.* **2019**, *148*, 68–74. [[CrossRef](#)]
15. Kocbek, E.; Garcia, H.A.; Hooijmans, C.M.; Mijatović, I.; Kržišnik, D.; Humar, M.; Brdjanovic, D. Effects of the sludge physical-chemical properties on its microwave drying performance. *Sci. Total. Environ.* **2022**, *828*, 154142. [[CrossRef](#)]
16. Yang, B.; Yuan, W.; Ma, B.; Zhang, Y.; Yang, Y. Study on the experiment in solution of electroplating pretreatment by microwave drying. *Environ. Sci. Technol.* **2013**, *26*, 1–3.
17. Kocbek, E.; Garcia, H.A.; Hooijmans, C.M.; Mijatović, I.; Lah, B.; Brdjanovic, D. Microwave treatment of municipal sewage sludge: Evaluation of the drying performance and energy demand of a pilot-scale microwave drying system. *Sci. Total. Environ.* **2020**, *742*, 140541. [[CrossRef](#)]
18. Zhou, W.; Zhang, L.; Peng, J.; Ge, Y.; Tian, Z.; Sun, J.; Cheng, H.; Zhou, H. Cleaner utilization of electroplating sludge by bioleaching with a moderately thermophilic consortium: A pilot study. *Chemosphere* **2019**, *232*, 345–355. [[CrossRef](#)]
19. Peng, Z.; Hwang, J.Y. Microwave-assisted metallurgy. *Int. Mater. Rev.* **2015**, *60*, 30–63. [[CrossRef](#)]
20. Du, J.; Gao, L.; Yang, Y.; Guo, S.; Chen, J.; Omran, M.; Chen, G. Modeling and kinetics study of microwave heat drying of low grade manganese ore. *Adv. Powder Technol.* **2020**, *31*, 2901–2911. [[CrossRef](#)]
21. Titze, T.; Lauerer, A.; Heinke, L.; Chmelik, C.; Zimmermann, N.E.R.; Keil, F.J.; Ruthven, D.M.; Kärger, J. Transport in nanoporous materials including MOFs: The applicability of Fick's laws. *Angew. Chem. Int. Ed.* **2015**, *54*, 14580–14583. [[CrossRef](#)] [[PubMed](#)]
22. Jia, S.; Cai, C. *Chemical Mass Transfer and Separation Process*; Chemical Industry Press: Beijing, China, 2001; pp. 32–33.
23. Zhou, Y.; Jian, Y. Mathematical modeling of thin-layer infrared drying of dewatered municipal sewage sludge (DWMSS). *Procedia Environ. Sci.* **2016**, *31*, 758–766. [[CrossRef](#)]
24. Midilli, A.; Kucuk, H.; Yapar, Z. A new model for single-layer drying. *Dry. Technol.* **2002**, *20*, 1503–1513. [[CrossRef](#)]
25. Balbay, A.; Sahin, O. Microwave drying kinetics of a thin-layer liquorice root. *Dry. Technol.* **2012**, *30*, 1503–1513. [[CrossRef](#)]
26. Danish, M.; Hu, J.; Zhou, P.; Lou, Z.; Qian, P. A new drying kinetic model for sewage sludge drying in presence of CaO and NaClO. *Appl. Therm. Eng.* **2016**, *106*, 141–152. [[CrossRef](#)]
27. Akaike, H. A new look at the statistical model identification. *IEEE Trans. Automat. Contr.* **1974**, *19*, 716–723. [[CrossRef](#)]
28. Yang, J.; Martens, W.N.; Frost, R.L. Transition of chromium oxyhydroxide nanomaterials to chromium oxide: A hot-stage Raman spectroscopic study. *J. Raman Spectrosc.* **2011**, *42*, 1142–1146. [[CrossRef](#)]

Disclaimer/Publisher's Note: The statements, opinions and data contained in all publications are solely those of the individual author(s) and contributor(s) and not of MDPI and/or the editor(s). MDPI and/or the editor(s) disclaim responsibility for any injury to people or property resulting from any ideas, methods, instructions or products referred to in the content.